Dynamics of microswimmers near a soft penetrable interface

Chao Feng,[1] John J. Molina,[1] Matthew S. Turner,[1,2] and Ryoichi Yamamoto[1,*]
[1]*Department of Chemical Engineering, Kyoto University, Kyoto 615-8510, Japan*
[2]*Department of Physics, University of Warwick, Coventry CV4 7AL, United Kingdom*

(Received 23 May 2022; accepted 22 November 2022; published 21 December 2022)

Few simulations exist for microswimmers near deformable interfaces. Here, we present numerical simulations of the hydrodynamic flows associated with a single microswimmer embedded in a binary fluid mixture. The two fluids demix, separated by a penetrable and deformable interface that we assume to be initially prepared in its planar ground state. We find that the microswimmer can either penetrate the interface, move parallel to it, or bounce back off it. We analyze how the trajectory depends on the swimmer type (pusher/puller) and the angle of incidence with respect to the interface. Our simulations are performed in a system with periodic boundary conditions, corresponding to an infinite array of fluid interfaces. A puller reaches a steady state in which it either swims parallel to the interface or selects a perpendicular orientation, repeatedly penetrating through the interface. In contrast, a pusher follows a bouncing trajectory between two interfaces. We discuss several examples in biology in which swimmers penetrate soft interfaces. Our paper can be seen as a highly simplified model of such processes.

DOI: 10.1103/PhysRevResearch.4.043202

I. INTRODUCTION

Microswimmers, including flagellated bacteria, such as *E. coli* [1] and motile, single-celled eukaryotes, such as *Chlamydomonas* [2], are common in biology and usually exist in complex fluid environments in nature. Systematic studies on the dynamics of microswimmers that can help us to understand their complex behaviors will, thus, allow us to further our understanding of basic biology and provide a guide for developing artificial micromachines. The latter could have great potential in various technological and biomedical applications [3,4], such as targeted drug delivery [5] or therapies using microrobots [6].

Although biological microswimmers are usually found in complex or inhomogeneous fluids, most theoretical/simulation studies on their dynamics have focused on simple homogeneous host environments [7–9]. Among the few works that have focused on the dynamics of microswimmers in inhomogeneous multiple-fluid systems, studies have usually focused on swimmers in the vicinity of solid/fluid interfaces [10–13] or liquid/gas interfaces [14]. These previous studies have revealed that microswimmers can be strongly influenced by liquid/solid and liquid/gas boundaries; they may loiter near, escape from, or glide along the boundary [11]. Over a longer timescale, circular motion at the boundary has even been observed with the swimming orientation determined by the boundary conditions [12].

Studies of swimmer dynamics in inhomogeneous systems with soft and/or penetrable interfaces are still limited in number due to the high associated computational costs [15,16]. In the present paper, we take a step toward understanding the behavior of microswimmers in complex environments by performing direct numerical simulation (DNS) of swimmers in a binary (Newtonian) fluid mixture. In particular, we fully account for the deformable and penetrable nature of the interface between the two phase-separated fluids.

This paper is organized as follows. First, we present the details of our theoretical model and numerical method. We then provide a comprehensive analysis of our DNS results in which we observe two distinct motions at the interface, depending on the type of swimmer and the incidence angle: (1) transmission across the interface and (2) bouncing back from the interface. Finally, we also present a detailed analysis and characterization of the resulting steady-state behavior.

II. SIMULATION METHODS

A. The squirmer model

To model microswimmers, the squirmer model is employed in this paper. It is a widely used model for a self-propelled particle in which the swimmer is represented as a spherical particle of radius a, with a modified stick boundary condition at its surface [7,17]. The slip velocity at a point $\boldsymbol{r}$ at the surface of the sphere is

$$\boldsymbol{u}^s(\vartheta) = \sum_{n=1}^{\infty} \frac{2}{n(n+1)} B_n P_n'(\cos\vartheta)\sin\vartheta\,\hat{\boldsymbol{\vartheta}}, \tag{1}$$

where $\vartheta = \cos^{-1}(\hat{\boldsymbol{r}}\cdot\hat{\boldsymbol{e}})$ is the polar angle between $\hat{\boldsymbol{r}}/|\boldsymbol{r}|$ the unit radial direction and $\hat{\boldsymbol{e}}$ the swimming direction, with $\hat{\boldsymbol{\vartheta}} = \hat{\boldsymbol{r}}\times(\hat{\boldsymbol{r}}\times\hat{\boldsymbol{e}})/\sin\vartheta$ the corresponding unit tangential vector. P_n' is the derivative of the Legendre

*ryoichi@cheme.kyoto-u.ac.jp

polynomial of the nth order, and B_n is the magnitude of the nth mode. Here, this surface velocity has only tangential polar components, responsible for the self-propulsion of the swimmer, and the radial and azimuthal contributions to this have been neglected [18,19].

In this paper, only the first two modes in Eq. (1) are retained

$$\boldsymbol{u}^s(\vartheta) = \left(B_1 \sin\vartheta + \frac{B_2}{2}\sin 2\vartheta\right)\hat{\boldsymbol{\vartheta}}. \tag{2}$$

The first term in Eq. (2) represents the swimmer's source dipole, and coefficient B_1 is physically related to the steady-state swimming velocity of the squirmer via $U_0 = 2/3B_1$. The second term corresponds to the force dipole and is proportional to the swimmer's stresslet. The ratio $\beta = B_2/B_1$ determines the squirmer's swimming type and its *strength*. When β is negative, the squirmer is a pusher and generates extensile flow fields in the direction of propulsion; when β is positive, the squirmer is a puller generating contractile flow fields. The marginal case of $\beta = 0$ corresponds to a neutral particle that swims with the potential flow in the surrounding fluid. In what follows, we will refer to the microswimmer with $|\beta| \leqslant 1$ as being weak whereas $|\beta| \geqslant 4$ as being strong. Different types of squirmers can be mapped to different kinds of microorganisms in nature.

B. Smoothed profile method

To simulate the dynamics of a swimming system with fully resolved hydrodynamic interactions, we employ the smoothed profile (SP) method [20]. In this method, all boundaries, including both fluid/solid and fluid/fluid boundaries, are considered to possess a finite interfacial thickness ξ. This greatly simplifies the modeling and improves the computational efficiency of the method as it avoids the need for complicated discretizations around the particles and the accompanying remeshing of other DNS approaches, such as spectral/hp element methods [21]. Fluid/solid boundaries are implicitly accounted for by introducing a phase field function $\phi(\boldsymbol{r})$, which is equal to 1 within solid domains (inside the squirmer particles), is equal to 0 within the fluid domain (outside of the squirmer particles), and smoothly varies between 0 and 1 across the interface. Thus, such an interface can be represented by the gradient of the phase field, which will be nonzero only within the interfacial domains.

A modified (incompressible) Navier-Stokes equation is employed as the governing equation for the total fluid velocity $\boldsymbol{u}$,

$$\rho(\partial_t + \boldsymbol{u}\cdot\nabla)\boldsymbol{u} = -\nabla p + \nabla\cdot\boldsymbol{\sigma} + \rho(\phi\boldsymbol{f}_p + \phi\boldsymbol{f}_{sq}), \tag{3}$$

$$\nabla\cdot\boldsymbol{u} = 0, \tag{4}$$

where $\boldsymbol{\sigma} = \eta(\nabla\boldsymbol{u} + \nabla\boldsymbol{u}^{\mathrm{T}})$ is the Newtonian stress tensor (viscosity η) and ρ is the fluid density. The term $\phi\boldsymbol{f}_p$ appearing on the right-hand side of Eq. (3) is introduced to enforce the rigidity of the particles; likewise, the term $\phi\boldsymbol{f}_{sq}$ is introduced to enforce the "squirming" boundary condition at the surfaces of the particles [Eq. (2)].

The total velocity is defined in terms of the fluid velocity field $\boldsymbol{u}_f$ and the particle velocity field $\boldsymbol{u}_p$ as

$$\boldsymbol{u} = (1-\phi)\boldsymbol{u}_f + \phi\boldsymbol{u}_p, \tag{5}$$

$$\phi\boldsymbol{u}_p = \sum_i \phi_i[\boldsymbol{V}_i + \boldsymbol{\Omega}_i\times\boldsymbol{R}_i], \tag{6}$$

where the first term $(1-\phi)\boldsymbol{u}_f$ represents the velocity field of the binary fluid, whereas the second term $\phi\boldsymbol{u}_p$ represents the particles' velocity field, which is defined in terms of the positions $\boldsymbol{R}_i$, velocities $\boldsymbol{V}_i$, and angular velocities $\boldsymbol{\Omega}_i$ of the particles (where i is the particle index).

The dynamics of the rigid particles are determined by the Newton-Euler equations of motion,

$$\dot{\boldsymbol{R}}_i = \boldsymbol{V}_i, \tag{7}$$

$$\dot{\boldsymbol{Q}}_i = \mathrm{skew}(\boldsymbol{\Omega}_i)\cdot\boldsymbol{Q}_i, \tag{8}$$

$$M_i\dot{\boldsymbol{V}}_i = \boldsymbol{F}_i^H + \boldsymbol{F}_i^C + \boldsymbol{F}_i^{\mathrm{ext}}, \tag{9}$$

$$\dot{\boldsymbol{J}}_i = \boldsymbol{N}_i^H + \boldsymbol{N}_i^{\mathrm{ext}}, \tag{10}$$

where M_i is the mass of particle i, $\boldsymbol{J}_i = \boldsymbol{I}_i\cdot\boldsymbol{\Omega}_i$ is its angular momentum ($\boldsymbol{I}_i$ is the moment of inertia), $\boldsymbol{Q}_i$ is the orientation matrix, and $\mathrm{skew}(\boldsymbol{\Omega}_i)$ is the skew-symmetric angular velocity matrix. The hydrodynamic forces and torques are given by $\boldsymbol{F}_i^H$ and $\boldsymbol{N}_i^H$, $\boldsymbol{F}_i^C$ represents direct particle-particle interactions ($\boldsymbol{N}_i^C = 0$), and $\boldsymbol{F}_i^{\mathrm{ext}}$ and $\boldsymbol{N}_i^{\mathrm{ext}}$ are the external forces and torques, respectively.

The accuracy of the SP method has been extensively studied in previous works [20,22–25]. For example, the friction and mobility tensors of nonspherical particle assemblies obtained from simulations at low Reynolds number (Re) are within $\lesssim 5\%$ of experimental values and high-precision solutions of the Stokes equation [24]. A similar degree of accuracy is found for the angular velocities of spherical particles under shear flow, for $\mathrm{Re} \lesssim 10$ [26], and the ζ potential of charged colloidal dispersions [27]. Likewise, simulation results for the terminal velocity of a rising droplet in a binary fluid (density ratio $\rho_A/\rho_B \leqslant 1$) were within $\lesssim 8\%$ of the theoretical predictions [25]. Finally, we note that these benchmark simulations were performed using relatively coarse resolutions for particles of size $a = 4$–5Δ with interfacial thickness $\xi = 2\Delta$ (Δ is the grid spacing).

C. Binary fluid model

The host fluid in our system is modeled as a phase-separating binary fluid mixture using the Cahn-Hilliard (CH) model, which, coupled with the Navier-Stokes hydrodynamics, yields the so-called model H [28,29]. We refer to the two phases of this binary mixture as fluids A and B. The spatial distributions of fluids A and B are given by order parameters $\psi_A(\mathbf{r})$ and $\psi_B(\boldsymbol{r})$, respectively, with $0 \leqslant \psi_\alpha \leqslant 1$. The composition of the fluid mixture is then determined by the order parameter $\psi(\boldsymbol{r})$,

$$\psi = \psi_A - \psi_B, \tag{11}$$

which takes a value of 1 in the A domain and a value of -1 in the B domain where the fractions of the constituent

components (fluid and particles) must sum to unity,

$$\psi_A + \psi_B + \phi = 1. \tag{12}$$

To account for the binary fluid nature of the host fluid, an additional force term is introduced in Eq. (3),

$$\rho(\partial_t + \boldsymbol{u}\cdot\nabla)\boldsymbol{u} = -\nabla p + \nabla\cdot\sigma - \psi\nabla\mu_\psi - \phi\nabla\mu_\phi + \rho(\phi\boldsymbol{f}_p + \boldsymbol{f}_{sq}), \tag{13}$$

where $\mu_\psi = \delta F/\delta\psi$ and $\mu_\phi = \delta F/\delta\phi$ are the locally defined chemical potentials with respect to ψ and ϕ, defined as functional derivatives of the Ginzburg-Landau free-energy F. The time evolution of ψ is given by the following CH equation:

$$\frac{\partial\psi}{\partial t} + (\boldsymbol{u}\cdot\nabla)\psi = \kappa\nabla^2\mu_\psi, \tag{14}$$

where κ is the mobility coefficient.

The free-energy F can be represented as follows:

$$F = \int d\boldsymbol{r}\Big[f(\psi) + \frac{\alpha}{2}(\nabla\psi)^2 + w\xi_p\psi(\nabla\phi)^2\Big]. \tag{15}$$

In Eq. (15), the first term $f(\psi) = \frac{1}{4}\psi^4 - \frac{1}{2}\psi^2$ represents the Landau double-well potential and has two minima at $\psi = 1$ and -1. The second term is the potential energy associated with the fluid A/B interface. The third term represents the particles' affinity for each of the fluid A/B phases. Thus, the chemical potentials are

$$\mu_\psi = f'(\psi) + \alpha\nabla^2\psi + w\xi_p(\nabla\phi)^2, \tag{16}$$

and

$$\mu_\phi = 2w\xi_p(\nabla\psi\cdot\nabla\phi + \psi\nabla^2\phi). \tag{17}$$

In the present paper, to keep the system as simple as possible, we assume that fluids A and B are immiscible but otherwise possess identical physical properties. In addition, we assume that the swimmers interact with the interface only hydrodynamically. Therefore, we set $w = 0$ in the present simulations.

III. RESULTS

In this paper, to investigate the dynamics of swimmers in inhomogeneous fluid systems, we focus on the dynamics of a single particle near a fluid-fluid interface. All simulations are conducted for an immiscible A/B fluid system in a rectangular computational domain with dimensions of $32\Delta \times 32\Delta \times 64\Delta$ with Δ being the grid spacing and unit of length. Periodic boundary conditions are established in all directions. Fluids A and B share all the same physical properties, such as density and viscosity, and are initially phase separated in the z direction (see Fig. 1).

The radius of the squirmer is $a = 4\Delta$. The fluid-fluid interface thickness ξ_f is of order unity with the present choice of $\alpha = 1$ in Eq. (15), and the particle-fluid interface thickness ξ_p is set to 2. The parameter B_1 in Eq. (2) is set to 0.015, corresponding to a single-particle steady-state velocity of $U_0 = 2/3B_1 = 0.01$. The mobility κ [Eq. (14)], the shear viscosity η, and the mass densities $\rho = \rho_A = \rho_B = \rho_p$ are all set to 1. Then, the particle Re is $\mathrm{Re} = \rho U_0 a/\eta = 0.08$, the Péclet number (Pe) is $\mathrm{Pe} = U_0 a/\kappa = 0.08$, and the Schmidt number (Sc) is $\mathrm{Sc} = \mathrm{Pe}/\mathrm{Re} = 1$.

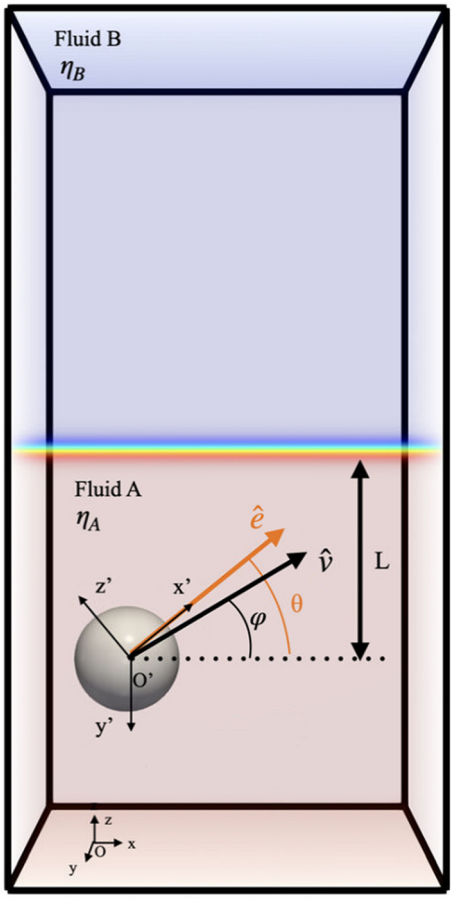

FIG. 1. Schematic of a single swimmer near a planar interface normal to $\hat{\boldsymbol{z}}$. The swimmer's squirming axis is $\hat{\boldsymbol{e}}$, and its angle with the interface defines the orientation of the particle, which is denoted as θ. The direction of motion is given by $\hat{\boldsymbol{v}}$ with relative angle to the interface φ.

A schematic of our system is given in Fig. 1, which shows a single swimmer near a fluid-fluid interface. The deformable interfaces are initially planar and are located at $z = 0$ and $z = 32\Delta$. The distance between the center of mass of the swimmer and the nearest interface is denoted by L. We choose $L = 16\Delta$ as the initial condition, unless noted otherwise. In all simulations the initial separation is large enough that no appreciable interfacial deformations are observed during the transient regime, before the swimmer reaches its steady-state velocity. The orientation of an interface is given by the vector $\hat{\boldsymbol{z}}$, $\hat{\boldsymbol{e}}$ denotes the swimmer's polar axis which is taken to be parallel to the body frame $\hat{\boldsymbol{x}}'$ axis, and $\hat{\boldsymbol{v}} = \boldsymbol{V}/|\boldsymbol{V}|$ denotes the swimmer's direction of motion. Since the initial velocity of the particle along the y axis is set to 0, the swimmer will move only on the x-z plane. The orientation $\theta = \arcsin(\hat{\boldsymbol{z}}\cdot\hat{\boldsymbol{e}})$ is defined as the angle between the polar axis and the interface, whereas the angle for the direction of motion is defined by $\varphi = \arcsin(\hat{\boldsymbol{z}}\cdot\hat{\boldsymbol{v}})$.

A. Motion near the interface

To examine the motions of microswimmers near an interface, we conduct a series of simulations in which a swimmer approaches the interface with different angles of approach

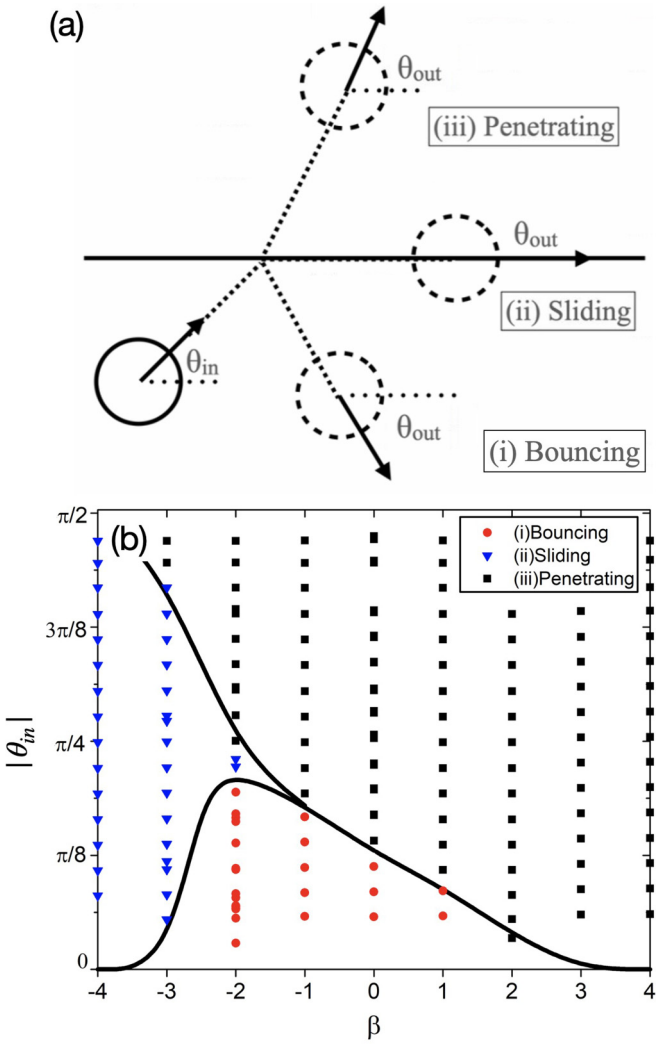

FIG. 2. (a) Graphical illustration of the three different swimming modes for a swimmer after a single collision with the interface. (b) Diagram showing how these modes depend on the initial incidence angle $|\theta_{\text{in}}|$ and swimming type β.

$\theta_{\text{in}} \in (0, \pi/2)$. As motions with the same initial angle magnitude $|\theta_{\text{in}}|$ are equivalent under a reflection symmetry, we will focus on the case where $\theta_{\text{in}} > 0$. After the swimmer leaves the interface, the outgoing angle is denoted by θ_{out}.

To understand the trajectories realised in our paper consider a swimmer that starts off in fluid A and approaches the interface . Three distinct "collision" modes are observed once the swimmer reaches the interface, namely, (i) "bouncing," (ii) "sliding," and (iii) "penetrating" motions as illustrated in Fig. 2(a). In case (i), the swimmer bounces back into fluid A, avoiding fluid B, after performing a significant rotation within the interfacial domain and leaving the interface with $\theta_{\text{out}} < 0$. In case (ii), the swimmer becomes trapped at the interface, swimming on the x-y plane with $\theta_{\text{out}} \simeq 0$. Finally, in case (iii), the swimmer passes through the interfacial barrier, swimming into fluid B with $\theta_{\text{out}} > 0$. See the movies in the supplemental material for animations of typical bouncing, sliding, and penetrating motion [30].

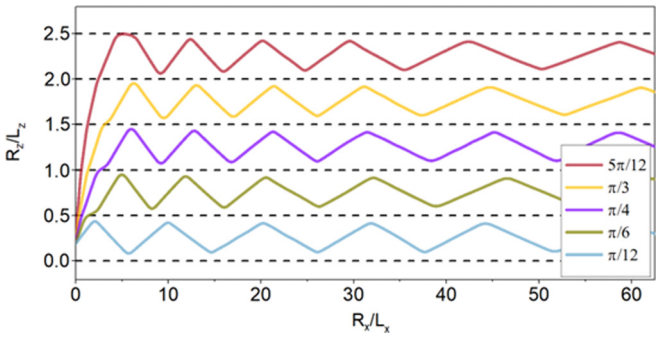

FIG. 3. Swimmer ($\beta = -2$) trajectories showing repeated collisions with the interfaces (dashed lines) for various initial angles θ_{in}. The swimmer position is shown in units of the system height L_z and width L_x as it moves in z (vertical) and x (horizontal), respectively.

We conducted simulations with various initial angles θ_{in} and swimming parameters β to construct a phase diagram for the three types of motions (i)–(iii), as shown in Fig. 2(b). For weak swimmers, whereas the swimming strength and swimmer type play a role, the dominant factor determining the nature of the motion at the interface is the initial angle. Generally, if $|\theta_{\text{in}}|$ is small, the swimmer will bounce back from the interface (i). If $|\theta_{\text{in}}|$ is large, the swimmer will swim across the interface (iii). For strong swimmers, pushers prefer to slide on the interface with their swimming orientation aligned with the boundary (ii), whereas pullers are more inclined to cross the interface (iii).

We also performed long-time simulations to study repeated collisions with interfaces. The particle orientation is allowed to evolve under these repeated collisions. Due to the periodic boundaries, the approaching/departing process is repeated with the swimmer colliding with the interface at an incoming angle θ_{in} equal to the outgoing angle θ_{out} of the previous collision. In the case of a pusher, a stable state of periodic back-and-forth motion between two interfaces is observed as shown in Fig. 3. The steady-state motion is the same for all $\beta = -2$ pushers, regardless of the initial angle. For a puller, the magnitude of angle θ increases during each pass, and finally, the swimmer reaches a steady state moving perpendicular to the interface. Thus, we consider that the swimmer type has a strong effect on the dynamics near fluid-fluid interfaces.

B. Swimmer types

We consider the swimmer dynamics as a function of β. Based on our simulation results, we obtain a map f relating the initial angle θ_{in} to the outgoing angle θ_{out} as presented in Fig. 4. To interpret this diagram for the case of multiple encounters, the θ_{out} achieved after one encounter should be read in as θ_{in} for the subsequent encounter. The penetrating mode and the bouncing mode are represented in black and red, respectively. For a neutral particle, orientation angle θ shows no change after the swimmer leaves the interface, regardless of its motion (bouncing or penetrating) as illustrated in Fig. 4(a).

Figures 4(b)–4(e) further illustrate the differences between pushers and pullers with the same $|\beta|$ values ($1 \leqslant |\beta| \leqslant 4$). Open symbols represent pullers, whereas filled symbols

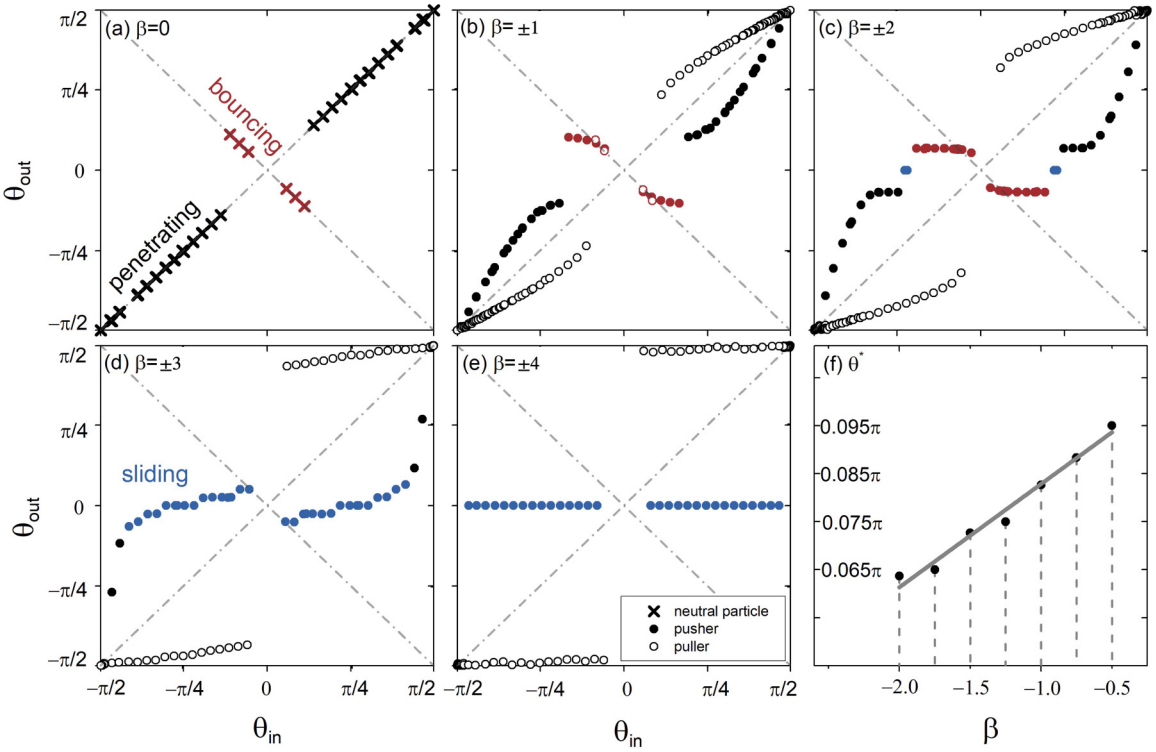

FIG. 4. Changes in the orientation angle θ for swimmers with various β values: (a) $\beta = 0$; (b) $\beta = \pm 1$; (c) $\beta = \pm 2$; (d) $\beta = \pm 3$; (e) $\beta = \pm 4$. Filled circles represent pushers, whereas empty circles represent pullers. Black indicates the crossing motion, and red indicates the bouncing motion. Blue represents the special case in which the swimmer ultimately swims along the interface. (f) The final fixed angles θ^* as a function of pushers' swimming strength β.

represent pushers. From these graphs, we can observe that the maps for swimmers with opposite values of β are nearly symmetric about the diagonal $\theta_{\text{out}} = \theta_{\text{in}}$, especially for the penetrating motion of weak swimmers (i.e., $\beta = \pm 1$). In other words, these maps are the inverse functions of each other. In general, swimmers with large initial angles, marked in black, swim across the interface. On the other hand, swimmers with small initial angles, marked in red, bounce back from the interface. However, the threshold angle that divides the bouncing and penetrating behaviors is different for different swimmers and depends on the β value. Even if pushers and pullers start from the same initial angle θ_{in} and exhibit the same swimming mode (penetrating or bouncing), their orientation angles will change in different ways. This is most easily seen from the penetrating trajectories of pullers and pushers with the orientation angle increasing for the former ($\theta_{\text{out}} > \theta_{\text{in}}$) and decreasing for the latter ($\theta_{\text{out}} < \theta_{\text{in}}$). For pullers ($\beta > 0$), only two types of motion, penetrating and bouncing motion, are observed. For pushers ($\beta < 0$), an additional sliding state is observed for $\beta \leqslant -3$, marked in blue. The swimmers are trapped by the interface, swimming along it, even though their orientations are not completely aligned with the interface (i.e., θ_{out} is not necessarily zero).

Figure 5 shows how orientation angle θ changes as a function of the distance from the nearest interface. Taking $L = 0$ as the dividing point of penetrating motion, and $\theta = 0$ as the dividing point for bouncing motion, we can decompose a complete interaction with the interface into two parts, corresponding to the approaching and departing processes. We note that these two processes show a clear symmetry about the interface ($L = 0$) for the neutral swimmers (c) trajectories, which is not observed for pushers (a-b) or pullers (d-e). Furthermore, for the case of pushers, the outgoing angle approaches a fixed value with the swimmers reaching a steady state in which they bounce back and forth periodically at this particular angle $\theta_{\text{out}} = -\theta_{\text{in}} = \theta^*$ [marked in yellow in Fig. 5(b)].

We note that the swimming strength also contributes to the hydrodynamic interactions near the interface. In particular, the change in orientation after crossing the boundary will be more pronounced for stronger swimmers. Thus, strong pullers will more quickly reach the stable state in which they swim perpendicular to the interface. For pushers for which the outgoing angle decreases, this can give rise to a sliding motion. The corresponding trajectories are marked in blue in Fig. 5(a). In such a case, the pusher can move along the interface with half of its body in fluid A and the other half in fluid B. This motion is reminiscent of the equatorial anchoring of Janus particles at an oil-water interface [31]. However, the former is due to the symmetry of the fluid system about the interface, whereas the latter is due to the symmetrical structure of the amphiphilic particles. Additionally, according to Fig. 2(b), the range of initial angles that can lead to this sliding motion increases as the swimming strength of the pusher increases.

We now consider the formation of different final stable states. Due to the symmetry considered in this paper, i.e., alternating fluid layers with identical properties for the two fluids, the swimmer trajectories show convergence after several interfacial interactions. We conduct a series of simulations in the bouncing regime for different initial orientations θ_0,

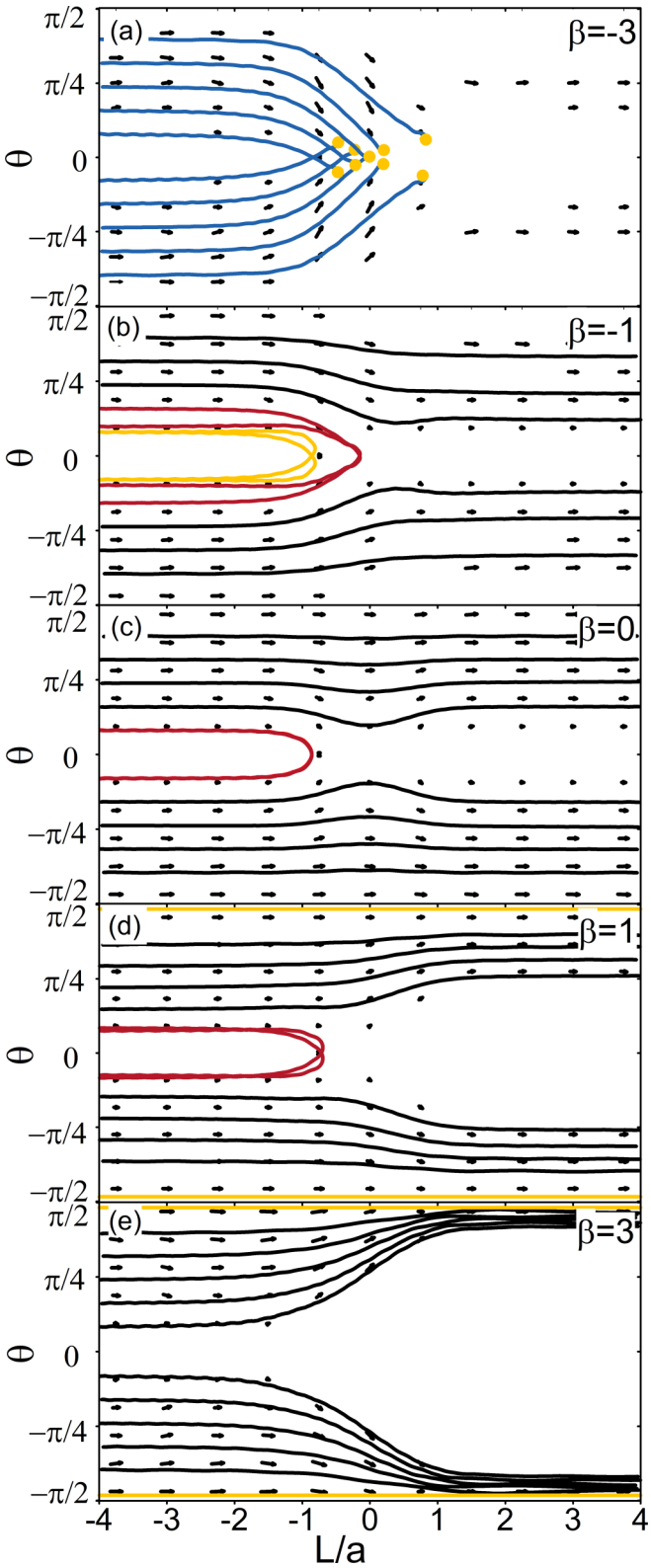

FIG. 5. Quiver plot showing the time evolution of orientation angle θ for swimmers with various β values: (a) and (b) pushers with (a) $\beta = -3$, (b) $\beta = -1$; (c) neutral particle; (d) and (e) pullers with (d) $\beta = 1$, (e) $\beta = 3$. Black and red lines indicate crossing and bouncing-back motions, respectively, whereas blue lines are used for swimmers that end up in the sliding motion, swimming parallel to the interface. Yellow indicates the steady state for swimmers with nonzero β.

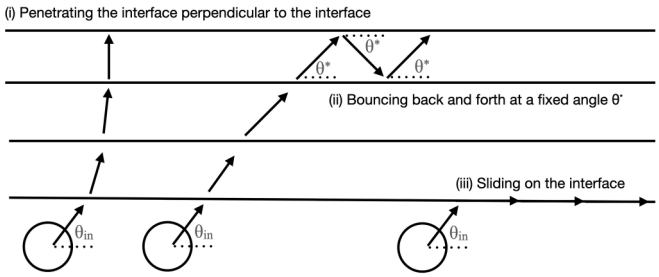

FIG. 6. Three types of stable states for swimmers: (i) A puller eventually swims perpendicular to the interface; (ii) a weak pusher eventually bounces back and forth between two interfaces at a fixed angle, while remaining in one of the fluid domains; (iii) a strong pusher eventually slides on the interface.

allowing the swimmer to collide with the interface several times. The orientation angle changes after each collision, approaching a steady-state value. Three distinct states are observed (see Fig. 6): (i) swimming perpendicular to the interface, (ii) bouncing back and forth at a fixed angle $\theta^\star$, or (iii) sliding on the interface. Multiple collisions can be considered as multiple iterations of the mapping $f(\theta_{\rm in}) \to \theta_{\rm out}$, which represents the change in angle after a single collision with an interface (Fig. 4). After the mth collision, the swimmer has an orientation $\theta^m_{\rm out}$, which will be the incidence angle for the next $(m+1)$ collision such that $\theta^{m+1}_{\rm in} = \theta^m_{\rm out}$. Figure 7 shows the changes in the swimmer orientation ($\beta = \pm 1$) after a sequence of $m = 6$ consecutive collisions. According to Fig. 7(a), the terminal angle of a weak puller will eventually converge to either $\pi/2$ or $-\pi/2$, regardless of the initial angle, marked yellow in Figs. 5(d) and 5(e). That is, after it has repeated the process of approaching an interface several times, a puller will eventually swim (i) perpendicular to the interface as shown in Fig. 6. A movie showing these repeated collisions and the resulting perpendicular alignment is given in the supplemental material [30].

For initial angles other than the boundary cases of $\theta = \pm\pi/2$, the terminal angle for a pusher will eventually converge (after repeated interfacial collisions) to an intersection point θ^* that is located in the bouncing motion regime as shown in Fig. 7(b). That is, pushers will always stabilize to a state in which they (ii) bounce back and forth at a fixed angle θ^* as shown in Fig. 6. A movie showing these repeated collisions and the resulting bouncing back motion is given in the supplemental material [30]. This fixed angle θ^* depends on the value of β as illustrated in Fig. 4(f).

In addition, for sufficiently strong pushers, (iii) sliding on the interface is also a possible steady state in which they are trapped at the interface without any displacement in the z axis and swim along it without any rotation [marked as yellow points in Fig. 5(a)], as shown in Fig. 6. A movie showing this sliding motion is given in the supplemental material [30].

IV. DISCUSSION

To the best of our knowledge, previous numerical studies of swimmer dynamics at interfaces [14,32] have usually considered only far-field hydrodynamics or nonpenetrable surfaces. In this paper we have considered a physical model in which

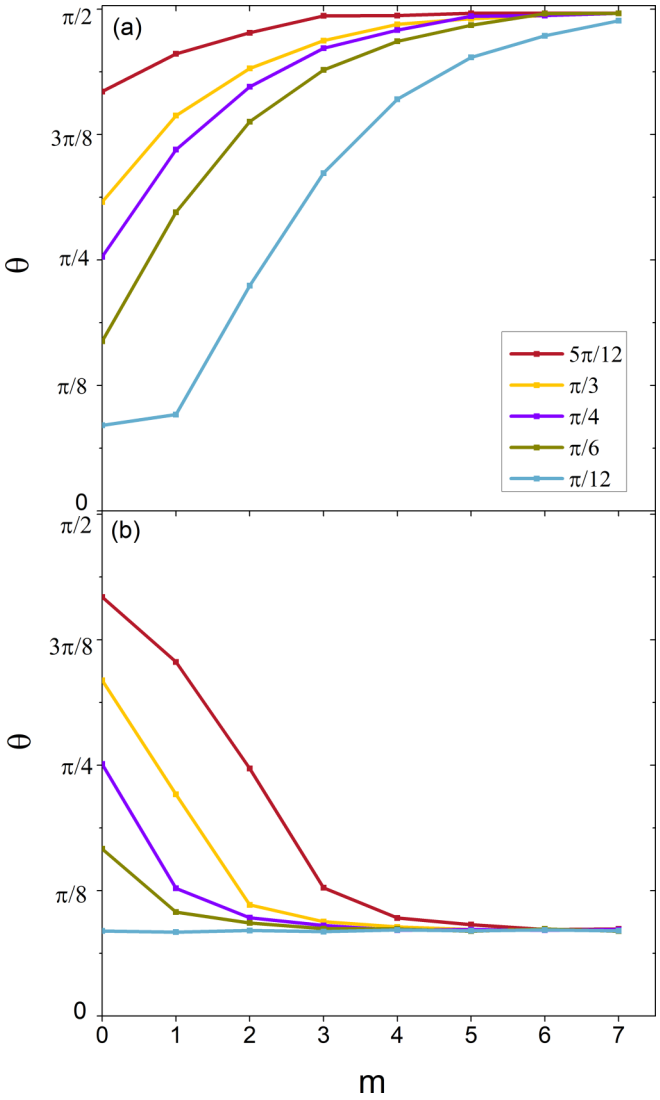

FIG. 7. The changes in the orientation θ for (a) puller ($\beta = 1$); (b) pusher ($\beta = -1$) after it collides with the interface m times.

swimmers interact with a soft, deformable, and penetrable interface. As a result, novel dynamics can be predicted and analyzed, such as the penetrating mode. In this mode, the swimmers pass through the interface and freely swim into the other fluid (no restrictions are imposed on its dynamics).

The work of Gidituri *et al.* is related to ours [33]. They investigate the reorientation dynamics of spherical microswimmers trapped at fluid-fluid interfaces. A sinusoidal dependence between the reorientation velocity Ω_F and angle θ is proposed based on their analytical arguments. Their simulation results are in agreement with this prediction $\Omega(\beta) = \hat{\Omega}_F(\beta)\sin 2\theta$ where the prefactor $\hat{\Omega}_F(\beta)$ depends linearly on β. To reproduce their conclusions, we also analyze our simulation data when swimmers cross the interface. As shown in Sec. B of the Supplemental Material [30], we are able to reproduce the sinusoidal dependence between the reorientation velocity Ω_F and the orientation θ. In addition, we also reproduce the linear dependence of the prefactor Ω_F on β. As expected (due to pusher/puller duality) for swimmers with opposite β values, these prefactors Ω_F have the same magnitude (opposite sign). Compared to the results of Gidituri *et al.* [33], the value we obtain for the slope of this prefactor is slightly decreased but shows good quantitative agreement (within error bars). This difference is reasonable, considering the fact that our particle is not fixed to the interface, the interface is deforming, we introduce a smooth profile to represent the particles, and we use a discretized spatial domain to numerically solve for the equations of motion.

Although the literature for bacteria swimming near fluid interfaces is less developed, the mode in which the swimmer slides on the interface has previously been reported by Deng *et al.* [34], who observed that *Pseudomonas aeruginosa* adsorbed onto an oil-water interface. This sliding motion was also studied by means of a general multipole-expansion-based singularity model for swimming microorganisms [35]. Both pushers and pullers were predicted to accumulate at an oil-water interface, giving rise to large density inhomogeneities in many-particle systems. Highly organized movements with remarkable large-scale patterns (i.e., networks, complex vortices, or swarms), which result from the collective dynamics of microswimmers, are observed [3,36]. In the present paper, we analyze only a single swimmer. This might help to explain why we predict instead that only strong pushers can be trapped by an interface. The work of Li and Ardekani [11] is probably the closest to ours, although they studied the motion of microswimmers near a solid wall. They found that a swimmer that was initially oriented toward the wall can escape (bounce back) if the strength of its squirming is sufficiently weak. However, they also reported another swimming mode in which very strong swimmers ($|\beta| > 7$) were observed to repeatedly bounce at the wall, which we do not observe in our simulations of a soft interface, although a hard/nonpenetrable interface is, of course, accessible within our methodology.

V. CONCLUSIONS

In this paper we analyze the dynamics of microswimmers in a binary fluid system. Our simulations are based on the SP method and the squirmer model. This allows accurate and efficient analysis of the dynamics near deformable fluid-fluid interfaces. Three qualitatively distinct dynamical modes emerge for swimmers approaching an interface, (i) penetrating, (ii) sliding, and (iii) bouncing. The dynamical properties depend on the swimmer type, the swimming strength, and the initial angle of approach. For a puller, the orientation angle is predicted to increase after the swimmer interacts with the interface. This will eventually reach $\pm\pi/2$ after repeated interfacial collisions, after which the puller will swim perpendicular to the interface. For a pusher the orientation angle instead approaches a fixed oblique angle $\theta^\star$, which can be increasing or decreasing, depending on whether the initial orientation was smaller or greater than this angle, respectively. As a consequence of this, we observe that most pushers will eventually exhibit a steady-state mode in which they bounce between two interfaces along trajectories inclined at angle θ^*. This steady-state angle θ^* is related to the swimmer type. For the case of a strong pusher, swimming parallel to the interface emerges as another possible dynamical mode.

Our results provide a detailed analysis of the hydrodynamic interactions of microswimmers with a deformable fluid-fluid

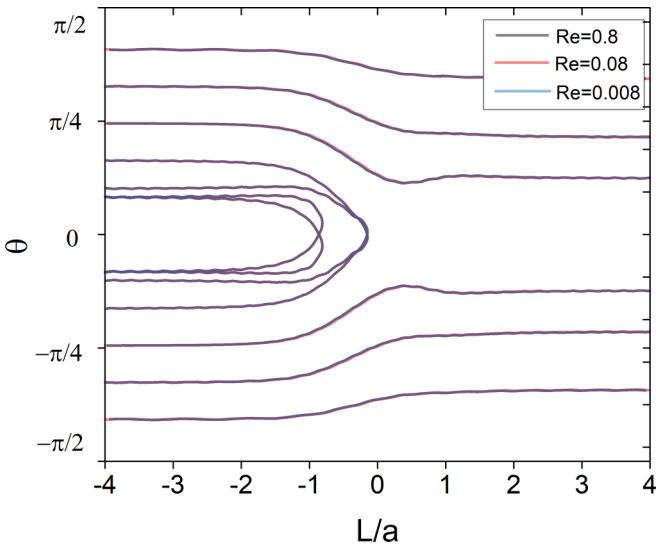

FIG. 8. Variation in orientation angle θ with different Res. Black lines, red lines, and blue lines are used for the cases with Re = 0.8, 0.08, and 0.008, respectively.

interface. This improves our understanding of microswimmer motion in environments involving soft interfaces, having some similarity with those found in biology. Our paper may also have some relevance in the context of bioengineering applications. For example, we could also incorporate additional features into our model, such as the nutrient chemotaxis. This represents an interesting aspect to be examined in future investigations.

ACKNOWLEDGMENTS

We express our gratitude to Dr. H. Ozaki and Dr. T. Aoyagi for their collaboration and outstanding contributions to the simulation software development. R.Y. acknowledges helpful discussions with Professors H. Tanaka and A. Furukawa. This work was supported by the Grants-in-Aid for Scientific Research (JSPS KAKENHI) under Grants No. JP 20H00129, No. 20H05619, and No. 20K03786 and by the NEDO Project (Project No. JPNP16010). This work was supported by JST, the establishment of university fellowships towards the creation of science technology innovation, Grant No. JPMJFS2123.

APPENDIX A: INERTIAL EFFECTS

All the simulations discussed above were conducted for a fixed Re (relative swimmer speed normalized with a momentum transport rate), a fixed Pe (relative swimmer speed normalized with a ψ transport rate), and a fixed Sc (relative momentum transport rate normalized with a ψ transport rate), which are set to Re = 0.08, Pe = 0.08, and Sc = 1, respectively, meaning that inertial effects are expected to be negligible. To examine the contribution of inertial effects to the swimmer dynamics, we also conducted some additional simulations for different values of Re and Pe. Figure 8 shows the variation in the orientation angle with the distance of the swimmer from the interface. The parameters used are the same as those in Fig. 5(f), except for the values of U_0. We compare three cases of pushers with Re = Pe = 0.008, 0.08, and 0.8 in Fig. 8 where it is seen that the three trajectories perfectly collapse on each other. This result indicates that the inertial effects are negligible in our present simulations. Although the effect of Sc is not considered in the present paper, it is also likely to contribute to the swimmer's dynamics as it approaches the interface. The exact mechanisms for this will require further investigation.

APPENDIX B: SOFTWARE

All simulations presented in this paper were conducted using the open-source version of the KAPSEL DNS software. KAPSEL has been developed in our laboratory to simulate the dynamics of solid particles dispersed in complex fluids. Detailed descriptions of KAPSEL are available online [37].

[1] H. C. Berg, *E. coli in Motion* (Springer, Berlin, 2004).
[2] K. Drescher, R. E. Goldstein, N. Michel, M. Polin, and I. Tuval, Direct Measurement of the Flow Field Around Swimming Microorganisms, Phys. Rev. Lett. **105**, 168101 (2010).
[3] J. Elgeti, R. G. Winkler, and G. Gompper, Physics of microswimmers—single particle motion and collective behavior: a review, Rep. Prog. Phys. **78**, 056601 (2015).
[4] E. Lauga, Bacterial hydrodynamics, Annu. Rev. Fluid Mech. **48**, 105 (2016).
[5] D. Laage and J. T. Hynes, A molecular jump mechanism of water reorientation, Science **311**, 832 (2006).
[6] H. Ceylan, I. C. Yasa, O. Yasa, A. F. Tabak, J. Giltinan, and M. Sitti, 3D-Printed Biodegradable Microswimmer for Theranostic Cargo Delivery and Release, ACS Nano **13**, 3353 (2019).
[7] M. T. Downton and H. Stark, Simulation of a model microswimmer, J. Phys.: Condens. Matter **21**, 204101 (2009).
[8] G. Volpe, S. Gigan, and G. Volpe, Simulation of the active brownian motion of a microswimmer, Am. J. Phys. **82**, 659 (2014).
[9] N. Oyama, J. J. Molina, and R. Yamamoto, Purely hydrodynamic origin for swarming of swimming particles, Phys. Rev. E **93**, 043114 (2016).
[10] G. Volpe, I. Buttinoni, D. Vogt, H.-J. Kümmerer, and C. Bechinger, Microswimmers in patterned environments, Soft Matter **7**, 8810 (2011).
[11] G.-J. Li and A. M. Ardekani, Hydrodynamic interaction of microswimmers near a wall, Phys. Rev. E **90**, 013010 (2014).
[12] K. Ishimoto and D. G. Crowdy, Dynamics of a treadmilling microswimmer near a no-slip wall in simple shear, J. Fluid Mech. **821**, 647 (2017).
[13] F. Fadda, J. J. Molina, and R. Yamamoto, Dynamics of a chiral swimmer sedimenting on a flat plate, Phys. Rev. E **101**, 052608 (2020).

[14] K. Ishimoto and E. A. Gaffney, Squirmer dynamics near a boundary, Phys. Rev. E **88**, 062702 (2013).

[15] V. A. Shaik and A. M. Ardekani, Motion of a model swimmer near a weakly deforming interface, J. Fluid Mech. **824**, 42 (2017).

[16] A. Daddi-Moussa-Ider, C. Kurzthaler, C. Hoell, A. Zöttl, M. Mirzakhanloo, M.-R. Alam, A. M. Menzel, H. Löwen, and S. Gekle, Frequency-dependent higher-order stokes singularities near a planar elastic boundary: Implications for the hydrodynamics of an active microswimmer near an elastic interface, Phys. Rev. E **100**, 032610 (2019).

[17] M. J. Lighthill, On the squirming motion of nearly spherical deformable bodies through liquids at very small Reynolds numbers, Commun. Pure Appl. Math. **5**, 109 (1952).

[18] O. S. Pak and E. Lauga, Generalized squirming motion of a sphere, J. Eng. Math. **88**, 1 (2014).

[19] T. Ishikawa, M. Simmonds, and T. J. Pedley, Hydrodynamic interaction of two swimming model micro-organisms, J. Fluid Mech. **568**, 119 (2006).

[20] R. Yamamoto, J. J. Molina, and Y. Nakayama, Smoothed profile method for direct numerical simulations of hydrodynamically interacting particles, Soft Matter **17**, 4226 (2021).

[21] X. Luo, M. R. Maxey, and G. E. Karniadakis, Smoothed profile method for particulate flows: Error analysis and simulations, J. Comput. Phys. **228**, 1750 (2009).

[22] R. Yamamoto, Y. Nakayama, and K. Kim, A smooth interface method for simulating liquid crystal colloid dispersions, J. Phys.: Condens. Matter **16**, S1945 (2004).

[23] Y. Nakayama and R. Yamamoto, Simulation method to resolve hydrodynamic interactions in colloidal dispersions, Phys. Rev. E **71**, 036707 (2005).

[24] J. J. Molina and R. Yamamoto, Direct numerical simulations of rigid body dispersions. I. mobility/friction tensors of assemblies of spheres, J. Chem. Phys. **139**, 234105 (2013).

[25] G. Lecrivain, Y. Kotani, R. Yamamoto, U. Hampel, and T. Taniguchi, Diffuse interface model to simulate the rise of a fluid droplet across a cloud of particles, Phys. Rev. Fluids **3**, 094002 (2018).

[26] J. J. Molina, K. Otomura, H. Shiba, H. Kobayashi, M. Sano, and R. Yamamoto, Rheological evaluation of colloidal dispersions using the smoothed profile method: Formulation and applications, J. Fluid Mech. **792**, 590 (2016).

[27] K. Kim, Y. Nakayama, and R. Yamamoto, Direct Numerical Simulations of Electrophoresis of Charged Colloids, Phys. Rev. Lett. **96**, 208302 (2006).

[28] N. Arai, S. Watanabe, M. T. Miyahara, R. Yamamoto, U. Hampel, and G. Lecrivain, Direct observation of the attachment behavior of hydrophobic colloidal particles onto a bubble surface, Soft Matter **16**, 695 (2020).

[29] G. Lecrivain, T. B. P. Grein, R. Yamamoto, U. Hampel, and T. Taniguchi, Eulerian/lagrangian formulation for the elasto-capillary deformation of a flexible fibre, J. Comput. Phys. **409**, 109324 (2020).

[30] See Supplemental Material S1–S5 at http://link.aps.org/supplemental/10.1103/PhysRevResearch.4.043202 for simulation movies of the various dynamical modes.

[31] B. J. Park, T. Brugarolas, and D. Lee, Janus particles at an oil–water interface, Soft Matter **7**, 6413 (2011).

[32] D. Pimponi, M. Chinappi, P. Gualtieri, and C. M. Casciola, Hydrodynamics of flagellated microswimmers near free-slip interfaces, J. Fluid Mech. **789**, 514 (2016).

[33] H. Gidituri, Z. Shen, A. Würger, and J. S. Lintuvuori, Reorientation dynamics of microswimmers at fluid-fluid interfaces, Phys. Rev. Fluids **7**, L042001 (2022).

[34] J. Deng, M. Molaei, N. G. Chisholm, and K. J. Stebe, Motile bacteria at oil–water interfaces: Pseudomonas aeruginosa, Langmuir **36**, 6888 (2020).

[35] N. Desai and A. M. Ardekani, Biofilms at interfaces: Microbial distribution in floating films, Soft Matter **16**, 1731 (2020).

[36] G. Gompper, C. Bechinger, S. Herminghaus, R. Isele-Holder, U. Benjamin Kaupp, H. Löwen, H. Stark, and R. G. Winkler, Microswimmers – from single particle motion to collective behaviour, Eur. Phys. J. Special Topics **225**, 2061 (2016).

[37] https://kapsel-dns.com